Access to the Active Site of Periplasmic Nitrate Reductase: Insights from Site-Directed Mutagenesis and Zinc Inhibition Studies†

Sébastien Dementin,*,‡,§ Pascal Arnoux,‡ Bettina Frangioni,§ Sandrine Grosse,‡ Christophe Léger,§ Bénédicte Burlat,§ Bruno Guigliarelli,§ Monique Sabaty,‡ and David Pignol*,‡

Laboratoire de Bioénergétique Cellulaire, CEA/Cadarache, DSV/IBEB/SBVME, 13108 St Paul lez Durance Cedex, France, and Laboratoire de Bioénergétique et Ingénierie des Protéines, CNRS, IBSM, 31 Chemin Joseph Aiguier, 13402 Marseille cedex 9, France

Received May 15, 2007; Revised Manuscript Received June 22, 2007

ABSTRACT: The periplasmic nitrate reductase (NapAB), a member of the DMSO reductase superfamily, catalyzes the first step of the denitrification process in bacteria. In this heterodimer, a di-heme NapB subunit is associated to the catalytic NapA subunit that binds a [4Fe-4S] cluster and a bis(molybdopterin guanine dinucleotide) cofactor. Here, we report the kinetic characterization of purified mutated heterodimers from *Rhodobacter sphaeroides*. By combining site-directed mutagenesis, redox potentiometry, EPR spectroscopy, and enzymatic characterization, we investigate the catalytic role of two conserved residues (M153 and R392) located in the vicinity of the molybdenum active site. We demonstrate that M153 and R392 are involved in nitrate binding: the V_m measured on the M153A and R392A mutants are similar to that measured on the wild-type enzyme, whereas the K_m for nitrate is increased 10-fold and 200-fold, respectively. The use of an alternative enzymatic assay led us to discover that NapAB is uncompetitively inhibited by Zn^{2+} ions ($K_i' = 1\ \mu M$). We used this property to further probe the active site access in the mutant enzymes. It is proposed that R392 acts as a filter by preventing a direct reduction of the Mo atom by small reducing molecules and partially protecting the active site against zinc inhibition. In addition, we show that M153 is a key residue mediating this inhibition likely by coordinating Zn^{2+} ions via its sulfur atom. This residue is not conserved in the DMSO reductase superfamily while it is conserved in the periplasmic nitrate reductase family. Zinc inhibition is therefore likely to be specific and restricted to periplasmic nitrate reductases.

Nitrate reductases are molybdenum-containing enzymes that catalyze the two-electron reduction of nitrate to nitrite. Three types of nitrate reductases have been described in bacteria. The three-subunit membrane anchored (Nar) and the dimeric periplasmic (Nap) enzymes are associated with respiratory transport pathways while the cytoplasmic enzyme (Nas) is involved in nitrate assimilation (*1*, *2*). The respiratory enzyme Nar catalyzes nitrate reduction with concomitant generation of proton motive force under anaerobic conditions (*3*), while the periplasmic enzyme Nap initiates the denitrification under both aerobic and anaerobic conditions (*4*). The latter group contains heterodimeric enzymes consisting of the subunits NapA and NapB. The large catalytic subunit NapA contains a MGD[1] cofactor and one [4Fe-4S] center. NapB is a di-heme cytochrome which serves as an electron transfer subunit between the membrane-anchored tetra-heme *c*-type cytochrome NapC and the catalytic subunit NapA (*5*).

The structure of NapA from *Desulfovibrio desulfuricans* was the first reported for a periplasmic nitrate reductase (*6*). The structure of the NapAB heterodimer from *Rhodobacter sphaeroides* was solved at 3.2 Å resolution and revealed the structural determinants required for optimal intermolecular electron transfer between both subunits of the complex (*7*). More recently, the 2.5 Å structure of *Escherichia coli* NapA has been solved and confirmed the previous structural analyzes (*8*). In both cases, NapA displays an α/β fold organized in four domains, all being involved in cofactor binding. The active site is a molybdenum atom hexacoordinated by the four dithiolene atoms of two MGD molecules, the sulfur atom of the Cys152 side chain, and one hydroxo/water ligand. A [4Fe-4S] cluster, located in proximity to the MGD, is involved in electron transfer. The structures of NapA from *D. desulfuricans*, *E. coli*, and *R. sphaeroides* are similar in terms of metal cofactor content and domain organization. In the structure of the heterodimer, the electron transfer subunit NapB embraces the NapA subunit in an

† This work was supported by the Commissariat à l'Energie Atomique, the program of nuclear toxicology and the ANR (PCV Program 2006−2009).

* To whom correspondence should be addressed. D.P.: CEA Cadarache, Bat 156 LBC/SBVME, 13115 Saint Paul lez Durance, France; tel, (33) 4 42 25 30 60; fax, (33) 4 42 25 47 01; e-mail, david.pignol@cea.fr. S.D.: BIP, CNRS, 31 chemin J. Aiguier, 13402 Marseille Cedex 9, France; tel, (33) 4 91 16 42 09; e-mail. dementin@ibsm.cnrs-mrs.fr.

‡ Laboratoire de Bioénergétique Cellulaire.

§ Laboratoire de Bioénergétique et Ingénierie des Protéines.

[1] Abbreviations: DMSO, dimethyl sulfoxide; ICP-MS, inductively coupled plasma mass spectrometry; NapAB, heterodimeric periplasmic nitrate reductase; MGD, molybdo-bis(molybdopterin guanine dinucleotide); Mo-co, molybdenum cofactor; MV, methyl viologen.

10.1021/bi700928m CCC: $37.00
Published on Web 08/03/2007

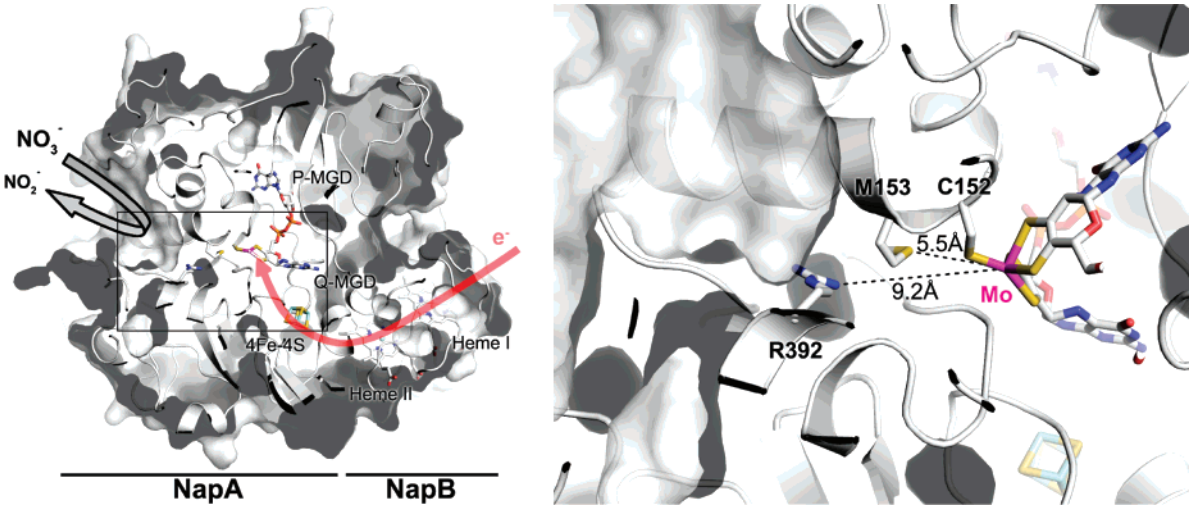

FIGURE 1: (A) The overall structure of the NapAB heterodimer from *R. sphaeroides*. The red arrow represents the electron transfer pathway from the distal heme of NapB to the catalytic molybdenum of NapA. The funnel-like substrate cavity extending from the surface to the active site is highlighted as a gray arrow. (B) View of the molybdenum active site, with M153 and R392, the two conserved residues mutated in this study.

extended conformation leading the heme II into the vicinity of the iron sulfur cluster of the catalytic subunit (*7*).

Spectroscopic, structural, and electrochemical studies have established a framework for understanding the reaction mechanism of NapAB (*9*). Kinetics experiments performed on purified NapA and NapAB from *R. sphaeroides* are consistent with a ping-pong mechanism: Mo^{VI} is reduced into Mo^{IV} prior to the oxo-transfer reaction which regenerates the oxidized form of the active site. NapB plays a key role in this process by increasing the electron transfer rate to the molybdenum (*7*). Although NapAB catalyzes *in vitro* the reduction of diverse substrates, such as selenate and tellurite, the catalytic efficiency is low in both cases (*10*). Thiocyanate and azide have been shown to act as competitive inhibitors with respect to nitrate by direct binding to the catalytic Mo via a sulfur atom (*11*). Cyanide, described as a noncompetitive inhibitor, was suggested to displace a terminal sulfur from the Mo coordination sphere (*11*).

To date, no enzymatic characterization has been performed on any purified periplasmic nitrate reductase and the precise functions of conserved residues located at the active site are still elusive. One article reported on mutagenesis studies of some residues around the molybdenum center in *Ralstonia eutropha* (*12*). Significantly, it was found that mutations R421E (equivalent of R392 in *R. sphaeroides*) and M183H (M153) led to a loss of activity. As informative as this study is, it has been carried out on periplasmic extracts, which precluded the authors from characterizing the kinetic and structural properties of the mutated proteins.

Recently, our laboratory engineered a *R. sphaeroides* strain able to produce large amounts of recombinant His-tagged wild-NapAB heterodimer. This system was successfully used to solve the first crystal structure of the wild-type NapAB complex (*7*). Here we report the first detailed mechanistic characterization of purified mutants that sheds light on the catalytic role of conserved residues located in the neighborhood of the catalytic molybdenum ion (Figure 1). We show that M153 and R392 are involved in substrate binding. Zn^{2+} ions efficiently inhibit the enzyme in an uncompetitive manner by binding in the active site *via* M153 in the presence of substrate. We also show that R392 acts as a filter that protects the active site from access to zinc and to small reducing molecules that can directly reduce the Mo ion.

EXPERIMENTAL PROCEDURES

Bacterial Strains, Plasmids, and Growth Conditions. Rhodobacter sphaeroides f. sp. denitrificans was grown at 30 °C in Hutner medium (*13*) under aerobic conditions (1.5 L of culture in 3 L Erlenmeyer flask, 150 rpm). *E. coli* strains were grown at 37 °C in Luria−Bertani medium. When necessary the medium was complemented with 1 μg mL^{-1} tetracycline for *R. sphaeroides* and 20 μg mL^{-1} tetracycline or 100 μg mL^{-1} ampicillin for *E. coli*.

Site-Directed Mutagenesis. QuickChange II XL Site-Directed Mutagenesis kit from Stratagene was used to generate point mutations into NapA. The size of the plasmid pMS617, a pRK415 derivative bearing *napAB* his-tagged (*10*), was too large, so a 2.4 kb *Xba*I-*Sac*I fragment containing the first 2392 bp of *napA* was cloned into pBluescript II KS. This plasmid was amplified using PfuUltra high fidelity DNA polymerase and two complementary oligonucleotides containing the desired mutation (in bold) flanked by unmodified nucleotide sequence. For mutant M153A the following primers were used: NAP M153A (5′-GCGCGCCACTGC**GCC**GCGTCGGCCGCCAC-3′) and rNAP M153A (5′-GTGGCGGCCGACGC**GGC**GCAGTG-GCGCGC-3′). For R392A mutant: NAP R392A (5′-CT-GCGGCACCGCG**GCC**GAGGTGGGCACC-3′) and rNAP R392A (5′-GGTGCCCACCTC**GGC**CGCGGTGCCGCAG-3′). After PCR amplification, the DNA was digested with *Dpn*I, which is specific for methylated DNA and is used to digest the parental DNA template. The nicked vector DNA incorporating the desired mutation was then transformed into *E. coli* DH5α competent cells. The insert was sequenced to verify that selected clones contain the desired mutation. This *Xba*I-*Sac*I fragment containing the mutation was then used to replace the *Xba*I-*Sac*I fragment of pMS617. The resulting plasmids were moved from *E. coli* to *R. sphaeroides* napA mutant MS523 (*4*) by standard procedure.

Protein Purification Methods. His-tagged wild-type and mutant NapAB complexes were overproduced and purified in a strain of *R. sphaeroides* deleted in nitrate reductase genes as previously decribed in ref *14*.

Nitrate/Reduced Methyl Viologen Assay. Nitrate reductase activity was assayed spectrophotometrically by measuring oxidation of reduced methyl viologen (MV) (ϵ_{600} nm = 13 mM^{-1} cm^{-1}). The reactions were carried out in anaerobic cuvettes at 30 °C in a 100 mM Tris/HCl buffer (pH 8) containing 2 mM MV and various concentrations of KNO_3 (final volume 4 mL). After flushing the cell with argon, MV was partially reduced to OD_{600nm} = 1.5−1.7 (115−130 μM reduced MV) with 10 to 20 μL of a freshly prepared 57 mM sodium dithionite solution. The reaction was started by addition of various quantities of purified wild-type or mutated NapAB complex. The slope of the recorded trace was used to calculate the oxidation rate of reduced MV.

Nitrite/Dithionite Assay. Nitrate reductase activity was alternatively followed by measuring production of nitrite using sodium dithionite instead of MV as the electron donor. The reactions were carried out in anaerobic cuvettes at 30 °C in a 100 mM Tris/HCl buffer (pH 8) containing various concentrations of KNO_3 (final volume 4 mL). After flushing the cell with argon, 5 to 20 μL of a freshly prepared 570 mM sodium dithionite solution was added. The reaction was started by the addition of the purified wild-type or mutated NapAB complex. Nitrite production was determined as described in ref *15* with slight modifications. This involves, first, the reaction in acid solution of a primary amine (sulfanilamide) with nitrite to form a diazonium salt which is then coupled to an aromatic amine to yield a red AZO dye. Concentration of this red dye can be determined spectrophotometrically at 540 nm. After 10 min of reaction, 0.5 mL of reaction mix was incubated for 15 min at room temperature with a solution containing 0.5 mL of H_2O, 0.25 mL of sulfanilamide 1% in HCl 3 N, and 0.25 mL of naphthylethylene diamine 0.01%. OD_{540nm} was measured and nitrite concentration was calculated using the slope of a linear sodium nitrite standard curve.

Inhibition Experiments. The inhibitory effect of Zn^{2+} on NapAB activity was studied with the two assays described above. The same procedure was followed with the anaerobic cuvettes containing $ZnSO_4$ over the range of 1−625 μM. Since Tris buffer binds most of the Zn^{2+} in our conditions, we estimated the free Zn^{2+} concentrations available in the solution using the equation $[Zn]_{free} = [Zn]_0/(1 + [Tris]_0/K_{tris})$ with a K_{tris} = 2.3 ± 0.2 mM, as previously determined at pH 7.5 by Gazaryan et al. (*16*). In our conditions (100 mM Tris/HCl buffer, pH 8), the value of $(1 + [Tris]_0/K_{tris})$ always equates 44.5.

Preparation and Reductase Activities of Periplasmic Extracts. Periplasmic extracts were prepared as followed. Cells from a 100 mL culture of *R. sphaeroides* f. sp. denitrificans supplemented with 20 mM KNO_3 or 20 mM DMSO were harvested, resuspended in 10 mL of Tris/HCl 50 mM pH 8, sucrose 0.45 M, EDTA 1.3 mM, and incubated with 1 mg/mL lysozyme for 1 h at 30 °C under gentle stirring. Cell pellet was removed by centrifugation at 8000 rpm at 4 °C for 10 min. The periplasmic fraction was collected by ultracentrifugation at 45000 rpm at 4 °C for 45 min. Proteins were quantified by the BCA assay (Pierce). DMSO reductase and nitrate reductase activities were determined at room temperature in the presence of 5 mM DMSO or 2.5 mM KNO_3 using MV as electron donor as described above.

Metal Content, Redox Titrations, and Spectroscopic Analysis. Metal content of NapAB mutants was measured by using ICP-MS analysis (spectrometer HP 4500, calibrated using external standard). Redox titrations were performed on a wide potential range in a specially designed anaerobic cell under argon atmosphere. Enzyme concentrations were in the 40−80 μM range in 20 mM Hepes, 100 mM NaCl buffer for M153A (pH 7.5) and R392A (pH 7.6) mutants, and 16 mM Hepes, 9 mM Tris, 80 mM NaCl (pH 7.2) for wild-type NapAB. A mixture of the following mediators was added, at 15 μM each: potassium ferricyanide, 1,4-benzoquinone, 2,5-dimethyl-*p*-benzoquinone, 1,2-naphthoquinone, phenazine methosulfate, phenazine ethosulfate, methylene blue, resorufine, indigo disulfonate, 2-hydroxy-(1,4)-naphthoquinone, phenosafranine, neutral red, methyl viologen. Redox potentials were adjusted with small additions of a 20 mM sodium dithionite or potassium ferricyanide solution and measured with a combined Pt−Ag/AgCl/KCl (3 M) microelectrode. Stable potentials were achieved in a few minutes, and samples were anaerobically transferred into calibrated EPR tubes which were rapidly frozen. All quoted potentials are given with respect to the standard hydrogen electrode. EPR experiments were performed on a Bruker ELEXSYS E500 spectrometer fitted with an Oxford Instrument ESR900 helium flow cryostat.

RESULTS

Enzyme Production and Cofactor Content. Overexpression in *Rhodobacter sphaeroides* and purification of the mutants led to a typical purification yield of about 1 mg per liter of cell culture. SDS gel electrophoresis revealed that the purity of the preparations was close to 100% in all cases and that no dissociation of the complex occurred in the course of the purification. No attempt was made to remove the 6His tag, and the preparations were directly concentrated prior to biophysical and biochemical experiments.

Metal content analyses confirmed that molybdenum is fully incorporated in all enzymes. The molar ratio 6 (Mo/Fe), which is equal theoretically to 100%, was determined by ICP-MS and found to be 94%, 91%, and 124% (±10%) in WT, M153A, and R392A enzymes, respectively. In the as prepared state of the WT enzyme, the two oxidized hemes gave at 15 K a single rhombic EPR signal at g = 2.92, 2.28, and 1.50 (Figure 2A). Upon reduction, this signal disappears progressively, and below −50 mV a rhombic $[4Fe\text{-}4S]^{+1}$ signal appears at g = 2.042, 1.947, 1.900 (Figure 2B). The two studied mutations have no significant effects on the EPR signatures of the hemes and of the [4Fe-4S] cluster, and spin intensity measurements performed in the fully oxidized and fully reduced states of the enzymes showed that the content of these centers is not affected. Taken together, these results indicate that the mutated enzymes keep their structural integrity and house all the cofactors, including the Mo-co. Moreover, the redox behaviors of the hemes and of the [4Fe-4S] center were determined by monitoring their EPR signal amplitude as a function of the redox potential. Although the mutated residues are rather distant from these centers, it appears clearly that their substitution can have a significant

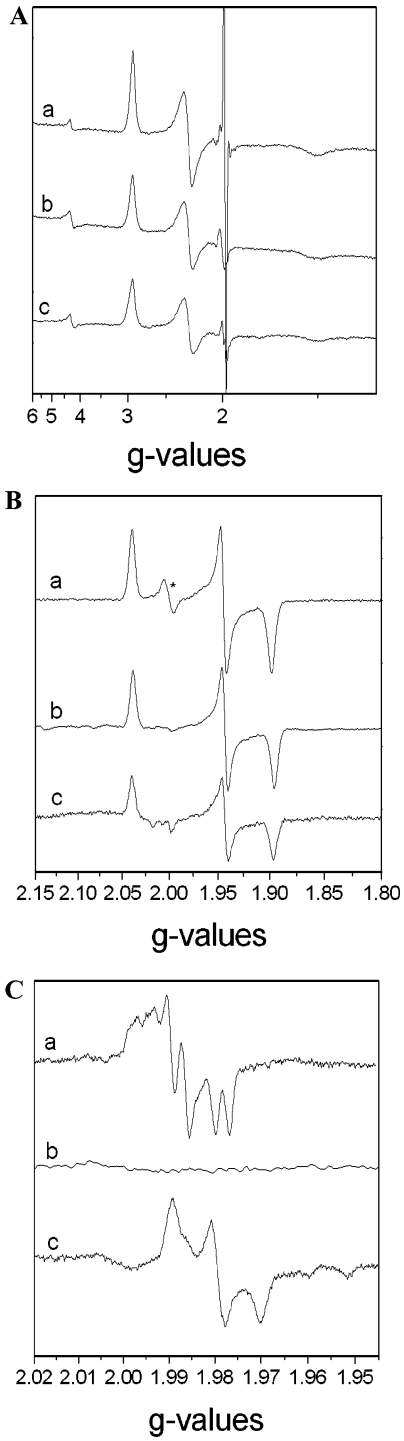

FIGURE 2: (A) X-band EPR spectra from hemes of oxidized NapAB (a) WT (as prepared), (b) R392A (as prepared), (c) M153A (as prepared). Recording conditions: temperature 15 K, microwave power 4 mW, modulation amplitude 1 mT. (B) X-band EPR spectra from $[4Fe4S]^{1+}$ of reduced NapAB (a) WT (−442 mV), (b) R392A (−369 mV), (c) M153A (−348 mV). Recording conditions: 15 K, microwave power 1 mW, modulation amplitude 0.5 mT. The signal marked with an asterisk come from the mediators. (C) X-band EPR spectra from Mo(V) of NapAB (a) WT (+232 mV), (b) R392A (−7 mV), (c) M153A (+39 mV). Recording conditions: 55 K, microwave power 1 mW, modulation amplitude 0.2 mT for a, 0.5 mT for b and c. Scan number: 1 for a and b, 16 for c.

effect on their redox properties (Table 1). The stronger effects were observed in the M153A mutant where the midpoint potential of the iron−sulfur center is decreased by about 100 mV, and that of the low potential heme shifts from −65 mV to −130 mV. Such indirect effects of amino acid replacement on the redox properties of a remote metal center were observed in various metalloproteins (*17*−*19*) and are considered to arise from weak distant induced conformation changes which modify polarity, solvent exposition, or hydrogen bond network around the center. Interestingly, the $[4Fe\text{-}4S]^{+1}$ EPR signal of the M153A mutant shows a broadening similar to that observed in the NapA enzyme expressed as a monomer and where the redox potential of the [4Fe-4S] cluster is decrease by 160 mV which supports this interpretation (*20*).

Table 1: Cofactor Reduction Potentials of WT and Mutants NapAB

enzyme	$E_{1/2}$ [4Fe4S] (mV)	$E_{1/2}$ heme I $E_{1/2}$ heme II (mV)	$E_{1/2}$ (Mo^{VI}/Mo^{V}) $E_{1/2}$ (Mo^{V}/Mo^{IV}) (mV)
WT	−80 ± 10	+80 ± 15 −65 ± 10	"high *g*" signal +570 ± 20 −225 ± 10
M153A	−180 ± 20	+75 ± 40 −130 ± 10	traces
R392A	−100 ± 10	+15 ± 15 −110 ± 10	no signal

In the as-prepared WT NapAB, the Mo-co is easily detected by EPR at 55 K as a Mo(V) species (Figure 2C). Its EPR spectrum is composed of a major "high *g*" rhombic signal (g_1 = 1.9987, g_2 = 1.9907, g_3 = 1.9810) which exhibits hyperfine couplings with two nonexchangeable protons (*8*). This species is stable on a very large potential range, the midpoint potential of the Mo(V)/Mo(IV) and Mo(VI)/Mo(V) being found at −225 mV and +570 mV, respectively. Depending on the enzyme preparation, a minor contribution of "very high *g*" Mo(V) signal (g_1 = 2.022, g_2 = 1.999, g_3 = 1.989) was also found. The total spin intensity of the Mo(V) signals represents between 0.1 and 0.2 spin per [4Fe-4S] cluster. Such a substoichiometry of the Mo(V) signal is a well-known feature of periplasmic nitrate reductases. In NapA from *Desulfovibrio desulfuricans* ATCC 27774 Mo(V) is described as accounting for 0.05 spin (*21*) while in *Paracoccus denitrificans* and *pantotrophus* this signal corresponds to 2.5−10% of total molybdenum (*22*, *23*). In *Escherichia coli*, no Mo(V) signal is described in the as-prepared state of NapA enzyme (*8*). However, in most cases the Mo(V) signal is increased after reduction with dithionite to a larger percentage (70−90% in the case of *Escherichia coli*). A substoichiometry of the Mo(V) signal is also often observed in multicenter molybdoenzymes of the DMSO family [see for example the studies of the membrane-bound nitrate reductase in refs *24* and *17* and ref *25*, the cytoplasmic nitrate reductase NarB (*26*), and the DMSO reductase (in as-prepared or dithionite-reduced states) (*27*, *28*)].

In contrast, no Mo(V) paramagnetic species was detected in R392A, even after careful examination in the large potential range. In M153A, a small amount (0.03 spin per [4Fe-4S] center) of a Mo(V) signal was observed between 0 and +200 mV. By comparison with the "high *g*" signal this signal has different *g*-values (g_1 = 1.9917, g_2 = 1.9818, g_3 = 1.9726) and it shows no resolved hyperfine structure (Figure 2C). This is surprising since the hyperfine couplings of the "high *g*" signal were proposed to arise from the β-CH_2 protons of the Mo cysteine ligand (*23*) which is not modified

Table 2: Kinetic Parameters of WT and Mutant Enzymes with Reduced MV or Dithionite as Electron Donor and in the Presence of Zinc

enzyme	$K_m^{KNO_3}$ (mM)	V_{max} (μmol min^{-1} mg^{-1})	$V_{dithionite}$[a] (μmol min^{-1} mg^{-1})
WT	0.41 ± 0.06	13.1 ± 0.7	0.22 ± 0.06
M153A	3.2 ± 0.7	13.2 ± 0.9	0.84 ± 0.32
R392A	65.5 ± 6.5	11.9 ± 0.4	3.69 ± 0.36

[a] Maximum specific activities measured with sodium dithionite as sole electron donor over the range 0−2.85 mM at 250 mM KNO_3.

by the mutation. As R392 and M153 are relatively distant from Mo ion (~9 and ~6 Å, respectively), the differences observed in the mutants for the stability and spectroscopic properties of the Mo(V) state suggest that mutations have brought about discrete structural rearrangements around the Mo-co. However, in native periplasmic nitrate reductases, the correspondence between the Mo(V) species identified by EPR and the catalytically relevant form of the active site is still unclear, and the physiological relevance of the "high *g*" Mo(V) species is not established. As a matter of fact, the V_m of the R392A and M153A mutants is identical to that of WT enzyme (see below). This indicates that in the mutants, the electron transfer through the hemes, the [4Fe4S] cluster to the Mo-co, and the catalytic process are not slowed down to the extent that they become rate-limiting for the reaction.

R392 and M153 Are Involved in Substrate Binding. The structures of the heterodimeric periplasmic nitrate reductases from *R. sphaeroides* and the monomeric nitrate reductase from *D. desulfuricans* show that a funnel-like cavity extending from the surface to the active site mediates the entrance of nitrate and its binding at the hydroxo/oxo ligand position of the molybdenum atom (Figure 1). Inside this channel, the side chain of two residues (R392 and M153) located in the vicinity of the Mo and conserved in the different species could play a role in binding and stabilizing the substrate.

The nitrate reductase activities were assayed spectrophotometrically for the purified complex NapAB and the R392A and M153A mutants, using methyl viologen at saturating concentration as electron source. In all cases, the kinetics were consistent with Michaelis−Menten behavior (see Supporting Information). The mutation of either the arginine or the methionine does not modify the maximal rate V_m (about 12−13 μmol min^{-1} mg^{-1}, see Table 2). However, the apparent affinity for nitrate is dramatically affected in both cases: the K_m for KNO_3 is increased 8-fold for the M153A mutant (3 mM) with respect to wild-type enzyme (0.4 mM), and the K_m value is as high as 65 mM when the guanidium side chain of residue 392 is removed. These results clearly demonstrate the role of M153 and R392 in promoting the substrate binding.

R392 Protects the Mo Site against Direct Reduction. Alternatively, nitrate reductase activities were followed by measuring the rate of nitrite formation in the presence of saturated concentration of substrate and using sodium dithionite instead of reduced MV as the electron donor (Table 2). Under such conditions, nitrite production catalyzed by WT NapAB is very slow (about 0.2 μmol min^{-1} mg^{-1}) suggesting that sodium dithionite can efficiently transfer electrons neither to the exposed heme I of NapB nor directly to the molybdenum active site of NapA. Direct electron transfer to the [4Fe4S] cluster is also unlikely since no nitrite

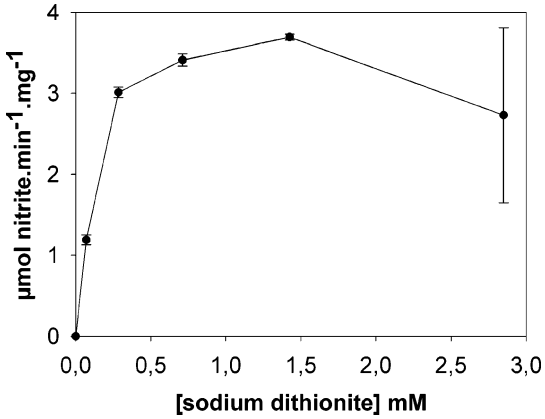

FIGURE 3: Nitrite production by R392A enzyme with sodium dithionite as electron donor. Sodium dithionite was varied from 0 to 2.85 mM at 250 mM KNO_3. Each point represents the mean of at least two independent experiments. For WT and M153A enzymes, in the same conditions, the maximum specific activities measured in the range of 0−2.85 mM sodium dithionite are 0.22 and 0.84 μmol min^{-1} mg^{-1}, respectively.

production could be detected with the purified wild-type NapA subunit under these conditions (data not shown). On the other hand, sodium dithionite is clearly a more efficient electron donor for the R392A mutant since under such conditions the maximal specific activity reaches 3.7 μmol min^{-1} mg^{-1} (Figure 3 and Table 2). Taking into account the very low or null activity of both WT NapAB and NapA in the presence of dithionite, together with the putative larger size of the substrate channel created by the removal of the arginine side chain in the mutant, we suggest that the production of nitrite catalyzed by R392A results from direct reduction of the molybdenum by dithionite. Thus, in addition to its role in binding nitrate, arginine 392 appears to protect the active site against direct reduction.

R392 Restricts the Zinc Access to the Active Site. M153 Plays a Key Role in Zn^{2+} Inhibition. In the course of this study, kinetic measurements initially performed using MV reduced by Zn(0) beads (as described in ref *29*) clearly suggested an inhibitory effect of this metal (data not shown). We confirmed that this effect was related to soluble Zn^{2+} ions produced upon reduction of MV by Zn(0). Since inhibition appeared to be different for the wild-type enzyme and the mutants, we exploited this behavior as an alternative approach to study the function of the mutated residues.

We first observed that adding EDTA, a Zn^{2+}-chelating molecule, in the reaction cuvette alleviated this inhibition and fully restored enzyme activity, suggesting a reversible inhibition (data not shown).

Kinetic analysis of the wild-type enzyme in the presence of various concentrations of KNO_3 and $ZnSO_4$ is presented in Figure 4 as Dixon (*30*) and Cornish-Bowden (*31*) plots. These representations provide a way to discriminate the type of inhibition and the K_i' constant. As a result, Zn^{2+} appears to be an uncompetitive inhibitor of NapAB with an inhibition constant of ~1 μM. In this type of inhibition, the effect of the inhibitor only occurs when the substrate is bound to the active site.

The same experiments were carried out on R392A and M153A mutants. In both cases, Zn^{2+} also acted as an uncompetitive inhibitor (Figure 4). Compared to the wild-type enzyme, the K_i' for R392A was considerably lowered

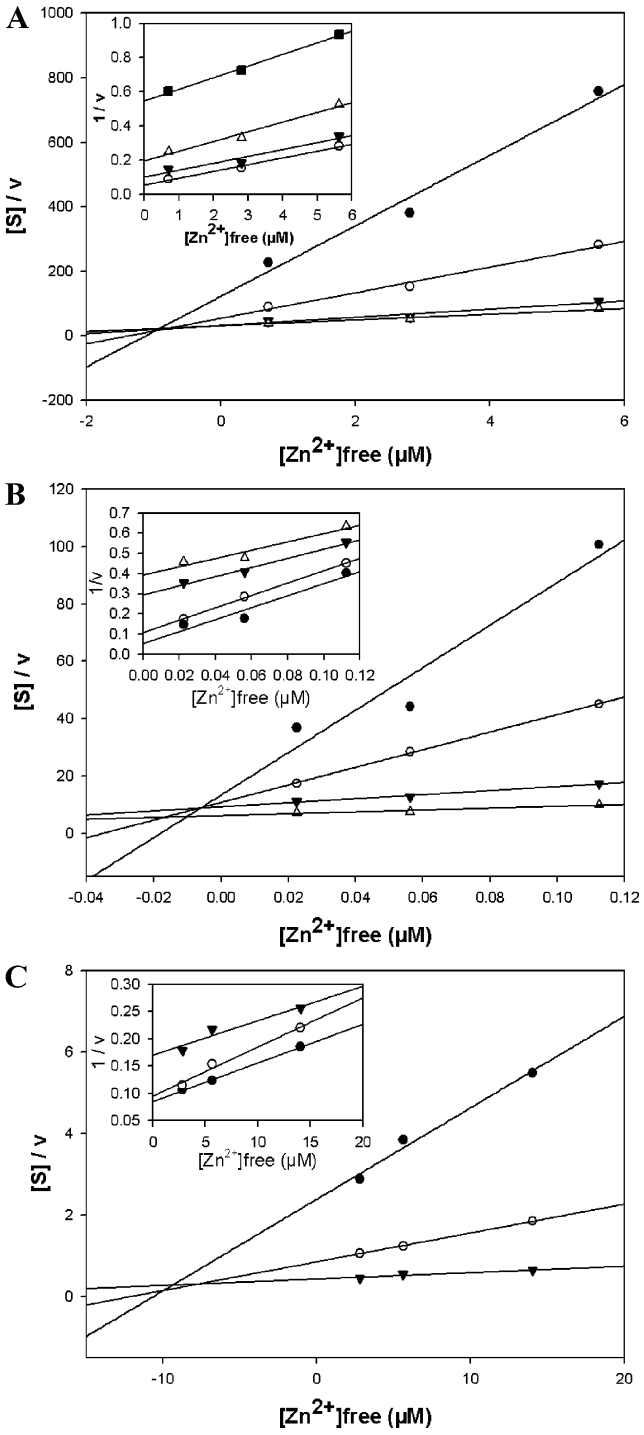

FIGURE 4: Kinetic analysis of the inhibition by $ZnSO_4$ of WT and mutant enzymes. The enzyme activities were measured with varying concentrations of $ZnSO_4$ at different nitrate concentrations. Data were plotted in Cornish-Bowden and (inset) Dixon plots. Each point represents the mean of at least two independent experiments (SD < 15%). (A) WT enzyme, $ZnSO_4$ was varied from 31 to 250 μM in the presence of 78.1 μM (■), 156.2 μM (△), 312.5 μM (▼), 1 mM (○), and 2.5 mM (●) KNO_3. (B) R392A enzyme, $ZnSO_4$ was varied from 1 to 5 μM in the presence of 15.6 mM (△), 31 mM (▼), 100 mM (○), and 250 mM (●) KNO_3. (C) M153A enzyme, $ZnSO_4$ was varied from 125 to 625 mM in the presence of 2.5 mM (▼), 10 mM (○), and 25 mM (●) KNO_3. $[Zn^{2+}]_{free}$ was calculated as described in Experimental Procedures. Lines were obtained by fitting the data using linear regression with the Sigma Plot 9.0 program (Systat Software, Inc). Intersection of the lines in the Cornish-Bowden plots provides a good estimation of the $-K_i'$ values ($K_i' \sim 1$, ~ 0.01, and ~ 10 μM for WT, R392A, and M153 enzymes, respectively).

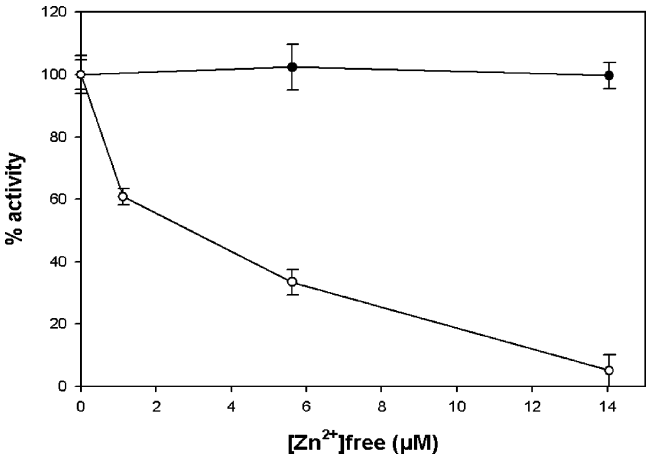

FIGURE 5: Effect of Zn^{2+} on the DMSO and nitrate reductase activities from a periplasmic extract of *R. sphaeroides*. Each point represents the mean of at least two independent experiments. $ZnSO_4$ was varied from 0 to 625 μM in the presence of 5 mM DMSO (●) or 2.5 mM KNO_3 (○). $[Zn^{2+}]_{free}$ was calculated as described in Experimental Procedures. Specific activities were calculated using the periplasmic protein concentration.

(below 10 nM) while that for M153A increased by 1 order of magnitude ($\sim$10 μM). These results revealed that the binding of Zn^{2+}, occurring inside the substrate-binding channel in the presence of nitrate, requires the M153 side chain and is facilitated by the absence of the guanidinium group of R392.

Zinc Inhibition Is Specific to Periplasmic Nitrate Reductases. In order to study the inhibitory effect of Zn^{2+} on the activity of other members of the DMSO reductase family, we measured the DMSO reductase activity of a periplasmic extract prepared from a wild-type strain. Cultures were previously grown in the presence of 20 mM DMSO to induce the synthesis of the DMSO reductase (*32*). As shown in Figure 5, Zn^{2+} up to 14 μM did not inhibit DMSO reductase activity while nitrate reductase activity was significantly affected. In addition, no Zn^{2+} inhibition was observed with the purified membrane-anchored nitrate reductase (NarGH) from *E. coli* (A. Magalon, personal communication). Thus, it seems that the inhibitory effect of Zn^{2+} ions is restricted to periplasmic nitrate reductase.

DISCUSSION

Detailed mechanistic studies using site-directed mutagenesis approaches have been reported for several members of the DMSO reductase family. However, no such work has been published for a periplasmic nitrate reductase. In this paper, we report the first detailed mechanistic characterization of purified mutants shedding light on the catalytic role of conserved residues located in the neighborhood of the catalytic molybdenum ion.

R392 is the only conserved basic residue in the funnel-like cavity connecting the solvent to the catalytic site. Since deletion of the guanidinium side chain of this residue affected only the K_m for nitrate but not the V_m, it is clear that R392 is not involved in the catalytic reduction of nitrate but promotes substrate binding. This result substantiates the mutagenesis study previously carried out on NapAB from *R. eutropha* (*12*). In this work, average specific activities monitored on periplasmic extracts prepared from cells producing mutated protein at the equivalent basic residue

(R421E and R421K) revealed a drastic loss of enzymatic activity compared to wild-type enzyme. Our results confirm a role of this arginine in substrate trafficking. It may directly interact with NO_3^- through electrostatic interaction or indirectly through electrostatic steering. Analysis of the substrate-free structures reveals that the geometry and the distances observed between R392 and the molybdenum atom (about 9.2 Å) are not compatible with the NO_3^- molecule being positioned at the sixth coordination site of the Mo and simultaneously interacting with the R392 guanidinium side chain (Figure 1). As a consequence, a direct R392−NO_3 binding would require a local conformation change that places the guanidinium side chain closer to both the substrate and the molybdenum atom. Such an arginine side chain rearrangement related to the presence or absence of bound substrate has been described in the catalytic cycle of sulfite oxidase (*33*).

The role of R392 was further investigated through nitrite/dithionite assays. Dithionite is a very poor electron donor to the wild-type monomeric or heterodimeric enzymes. Surprisingly, the deletion of the R392 side chain remarkably increases the nitrite production rate when dithionite is used as the sole electron source. This result is consistent with a direct reduction of the active site (probably the molybdenum atom) by dithionite in the mutant, made possible by the enlargement of the substrate-binding channel. In addition to stabilizing substrate at the active site, R392 is also likely to be involved in preventing the direct interaction of small redox molecules (including dithionite) with the catalytic Mo, thus making the electrons flow through the solvent exposed heme and the [4Fe4S] cluster during catalysis.

Another insight in the study of periplasmic nitrate reductase comes from our characterization of the inhibitory behaviors of zinc. We clearly demonstrate that Zn^{2+} acts on the *R. sphaeroides* periplasmic nitrate reductase as uncompetitive inhibitor with respect to nitrate ($K_i' \sim 1$ μM). This type of inhibition implies that the substrate binding unmasks the Zn^{2+} binding site. The characterization of M153A and R392A mutants' Zn^{2+} inhibition is very informative regarding the localization of the inhibitor binding site and the inhibitory mechanism. First, the R392A mutant is considerably more affected than the wild-type enzyme ($K_i' \sim 10$ nM vs $K_i' \sim 1$ μM). Taking into account that the deletion of the guanidinium side chain in the mutant facilitates the access of small molecules to the active site, Zn^{2+} could easily bind near the active site. The substrate interaction with the sixth coordination site of the Mo ion, coming with a local conformational change of R392, could be related to the uncompetitive character of zinc inhibition. Indeed, a putative guanidinium side chain movement could accompany the nitrate to the molybdenum ion and concomitantly unmask the Zn^{2+} binding site. Alternatively, the uncompetitive inhibitory effect of zinc, which requires the previous binding of the substrate at the active site, could reflect a direct Zn^{2+}−NO_3^- interaction. These issues should be clarified by solving the structure of a periplasmic nitrate reductase in the presence of both nitrate and zinc ions. Remarkably, the M153A mutant is significantly less sensitive to Zn^{2+} ions ($K_i' \sim 10$ μM) than the WT, demonstrating that the methionine is an important structural determinant of inhibitor binding. The sulfur of methionyl residues is known to react with metal ions. It participates for instance in the coordination of (i) the heme irons of cytochrome c_{553} from *Bacillus pasteuri* (*34*) and of mutants of *E. coli* cytochrome *b*562 (*35*); (ii) the copper in the plastocyanin from *Synechocystis* sp. PCC 6803 (*36*), the CuA domain of *Thermus thermophilus* ba_3-type cytochrome *c* oxidase (*37*) and in the *Haemophilus ducreyi* Cu, Zn superoxide dismutase (*38*). A role of Cu^{2+} and/or Zn^{2+} binding via sulfur of a methionyl residue was evidenced for prion peptide P106-126 aggregation and neurotoxicity (*39*). In the light of these examples, we propose that Zn^{2+} inhibition of the periplasmic nitrate reductase occurs via its coordination to the sulfur of M153. This methionyl residue is absent in the membrane-bound nitrate reductase of *E. coli* and the DMSO reductase from *R. sphaeroides*, and indeed, the activities of both enzymes are not affected by Zn^{2+} ions.

The inhibitory effect of Zn^{2+} ions on bacterial periplasmic nitrate reductase is an unexpected observation, although *in vivo* and *in vitro* studies have already described such an effect on eukaryotic nitrate reductase activities. Indeed, Mathys (*40*) described a strong inhibition of nitrate reductase activity in leaves of a zinc-resistant *Silene cucubalus* strain population when $ZnSO_4$ was added in the reaction medium (IC_{50} 6μM). Nitrate reductase from *Aspergillus* sp. was shown to be inhibited by $ZnSO_4$ *in vitro* ($IC_{50} \sim 6$ μM). More recently, Tripathi et al. determined that the nitrate reductase activity of green algua *Scenedesmus* sp. exposed to Zn^{2+} stress was reduced (*41*). No precise kinetic characterization of the inhibitory effects has ever been reported. The structure of the eukaryotic nitrate reductase from *Pichia angusta* displays an overall fold that differs from that of the dissimilatory bacterial enzymes, but with striking similarities at the active site: a Mo-ligating cysteine surrounded by similar type of residues (M427 and R144 in *P. angusta* numbering) (*42*). Since zinc inhibition has been described *in vitro* for eukaryotic nitrate reductases, and is now clearly evidenced for the bacterial periplasmic enzyme, a similar mechanism of Zn^{2+} binding in eukaryotic and periplasmic nitrate reductase active sites may be hypothesized. Preliminary assays performed with $CdCl_2$, also described as an inhibitor of eukaryotic nitrate reductase, revealed that Cd^{2+} ions inhibit the periplasmic nitrate reductase in a way similar to Zn^{2+}. As these inhibitions are efficient and seem specific to periplasmic nitrate reductase, their physiological relevance in prokaryotes is now under study in order to determine how these cations affect the enzyme *in vivo* and how the cell accommodates such metal stress.

ACKNOWLEDGMENT

We thank Dr. J. Lavergne for the critical review of the manuscript.

SUPPORTING INFORMATION AVAILABLE

Kinetic analysis of the nitrate reductase activity of WT, M153A, and R392A enzymes. This material is available free of charge via the Internet at http://pubs.acs.org.

REFERENCES

1. Bertero, M. G., Rothery, R. A., Palak, M., Hou, C., Lim, D., Blasco, F., Weiner, J. H., and Strynadka, N. C. (2003) Insights into the respiratory electron transfer pathway from the structure of nitrate reductase A, *Nat. Struct. Biol. 10*, 681−687.

2. Richardson, D. J., Berks, B. C., Russell, D. A., Spiro, S., and Taylor, C. J. (2001) Functional, biochemical and genetic diversity of prokaryotic nitrate reductases, *Cell. Mol. Life Sci. 58*, 165−178.
3. Blasco, F., Guigliarelli, B., Magalon, A., Asso, M., Giordano, G., and Rothery, R. A. (2001) The coordination and function of the redox centres of the membrane-bound nitrate reductases, *Cell. Mol. Life Sci. 58*, 179−193.
4. Sabaty, M., Schwintner, C., Cahors, S., Richaud, P., and Vermeglio, A. (1999) Nitrite and nitrous oxide reductase regulation by nitrogen oxides in *Rhodobacter sphaeroides* f. sp. denitrificans IL106, *J. Bacteriol. 181*, 6028−6032.
5. Cartron, M. L., Roldan, M. D., Ferguson, S. J., Berks, B. C., and Richardson, D. J. (2002) Identification of two domains and distal histidine ligands to the four haems in the bacterial c-type cytochrome NapC; the prototype connector between quinol/quinone and periplasmic oxido-reductases, *Biochem. J. 368*, 425−432.
6. Dias, J. M., Than, M. E., Humm, A., Huber, R., Bourenkov, G. P., Bartunik, H. D., Bursakov, S., Calvete, J., Caldeira, J., Carneiro, C., Moura, J. J., Moura, I., and Romao, M. J. (1999) Crystal structure of the first dissimilatory nitrate reductase at 1.9 Å solved by MAD methods, *Structure 7*, 65−79.
7. Arnoux, P., Sabaty, M., Alric, J., Frangioni, B., Guigliarelli, B., Adriano, J. M., and Pignol, D. (2003) Structural and redox plasticity in the heterodimeric periplasmic nitrate reductase, *Nat. Struct. Biol. 10*, 928−934.
8. Jepson, B. J. N., Mohan, S., Clarke, T. A., Gates, A. J., Cole, J. A., Butler, C. S., Butt, J. N., Hemmings, A. M., and Richardson, D. J. (2007) Spectropotentiometric and structural analysis of the periplasmic nitrate reductase from *Escherichia coli*, *J. Biol. Chem. 282*, 6425−6437.
9. Frangioni, B., Arnoux, P., Sabaty, M., Pignol, D., Bertrand, P., Guigliarelli, B., and Leger, C. (2004) In *Rhodobacter sphaeroides* respiratory nitrate reductase, the kinetics of substrate binding favors intramolecular electron transfer, *J. Am. Chem. Soc. 126*, 1328−1329.
10. Sabaty, M., Avazeri, C., Pignol, D., and Vermeglio, A. (2001) Characterization of the reduction of selenate and tellurite by nitrate reductases, *Appl. Environ. Microbiol. 67*, 5122−5126.
11. Butler, C. S., Charnock, J. M., Garner, C. D., Thomson, A. J., Ferguson, S. J., Berks, B. C., and Richardson, D. J. (2000) Thiocyanate binding to the molybdenum centre of the periplasmic nitrate reductase from *Paracoccus pantotrophus*, *Biochem. J. 352 Pt 3*, 859−864.
12. Hettmann, T., Siddiqui, R. A., Frey, C., Santos-Silva, T., Romao, M. J., and Diekmann, S. (2004) Mutagenesis study on amino acids around the molybdenum centre of the periplasmic nitrate reductase from *Ralstonia eutropha*, *Biochem. Biophys. Res. Commun. 320*, 1211−1219.
13. Clayton, R. K. (1960) Physiology of induced catalase synthesis in *Rhodopseudomonas spheroids*, *J. Cell. Comp. Physiol. 55*, 1−7.
14. Pignol, D., Adriano, J. M., Fontecilla-Camps, J. C., and Sabaty, M. (2001) Crystallization and preliminary X-ray analysis of the periplasmic nitrate reductase (NapA-NapB complex) from *Rhodobacter sphaeroides* f. sp. denitrificans, *Acta Crystallogr., Sect. D: Biol. Crystallogr. 57*, 1900−1902.
15. Nicholas, D. J. D., and Nason, A. (1957) Determination of nitrate and nitrite, *Methods Enzymol. 3*, 981−984.
16. Gazaryan, I. G., Krasnikov, B. F., Ashby, G. A., Thorneley, R. N., Kristal, B. S., and Brown, A. M. (2002) Zinc is a potent inhibitor of thiol oxidoreductase activity and stimulates reactive oxygen species production by lipoamide dehydrogenase, *J. Biol. Chem. 277*, 10064−10072.
17. Magalon, A., Asso, M., Guigliarelli, B., Rothery, R. A., Bertrand, P., Giordano, G., and Blasco, F. (1998) Molybdenum cofactor properties and [Fe-S] cluster coordination in *Escherichia coli* nitrate reductase A: investigation by site-directed mutagenesis of the conserved his-50 residue in the NarG subunit, *Biochemistry 37*, 7363−7370.
18. Kyritsis, P., Kummerle, R., Huber, J. G., Gaillard, J., Guigliarelli, B., Popescu, C., Munck, E., and Moulis, J. M. (1999) Unusual NMR, EPR, and Mossbauer properties of *Chromatium vinosum* 2[4Fe-4S] ferredoxin, *Biochemistry 38*, 6335−6345.
19. Lanciano, P., Magalon, A., Bertrand, P., Guigliarelli, B., and Grimaldi, S. (2007) High-Stability Semiquinone Intermediate in Nitrate Reductase A (NarGHI) from *Escherichia coli* Is Located in a Quinol Oxidation Site Close to Heme b(D), *Biochemistry 46*, 5323−5329.
20. Frangioni, B. (2006) in *Etude fonctionnelle de la nitrate périplasmique de Rhodobacter sphaeroides par spectroscopie RPE et électrochimie directe*, Thesis, Université Aix marseille I, France.
21. Gonzalez, P. J., Rivas, M. G., Brondino, C. D., Bursakov, S. A., Moura, I., and Moura, J. J. G. (2006) EPR and redox properties of periplasmic nitrate reductase from *Desulfovibrio desulfuricans* ATCC 27774, *J. Biol. Inorg. Chem. 11*, 609−616.
22. Butler, C. S., Charnock, J. M., Bennett, B., Sears, H. J., Reilly, A. J., Ferguson, S. J., Garner, C. D., Lowe, D. J., Thomson, A. J., Berks, B. C., and Richardson, D. J. (1999) Models for molybdenum coordination during the catalytic cycle of periplasmic nitrate reductase from *Paracoccus denitrificans* derived from EPR and EXAFS spectroscopy, *Biochemistry 38*, 9000−9012.
23. Butler, C. S., Fairhurst, S. A., Ferguson, S. J., Thomson, A. J., Berks, B. C., Richardson, D. J., and Lowe, D. J. (2002) Mo(V) co-ordination in the periplasmic nitrate reductase from *Paracoccus pantotrophus* probed by electron nuclear double resonance (ENDOR) spectroscopy, *Biochem. J. 363*, 817−823.
24. Guigliarelli, B., Asso, M., More, C., Augier, V., Blasco, F., Pommier, J., Giordano, G., and Bertrand, P. (1992) EPR and redox characterization of iron-sulfur centers in nitrate reductases A and Z from *Escherichia coli*. Evidence for a high-potential and a low-potential class and their relevance in the electron-transfer mechanism, *Eur. J. Biochem. 207*, 61−68.
25. Vincent, S. P., and Bray, R. C. (1978) Electron-paramagnetic-resonance studies on nitrate reductase from *Escherichia coli* K12, *Biochem. J. 171*, 639−647.
26. Jepson, B. J. N., Anderson, L. J., Rubio, L. M., Taylor, C. J., Butler, C. S., Flores, E., Herrero, A., Butt, J. N., and Richardson, D. J. (2004) Tuning a nitrate reductase for function-The first spectropotentiometric characterization of a bacterial assimilatory nitrate reductase reveals novel redox properties, *J. Biol. Chem. 279*, 32212−32218.
27. Bastian, N. R., Kay, C. J., Barber, M. J., and Rajagopalan, K. V. (1991) Spectroscopic studies of the molybdenum-containing dimethyl sulfoxide reductase from *Rhodobacter sphaeroides* f. sp. denitrificans, *J. Biol. Chem. 266*, 45−51.
28. Benson, N., Farrar, J. A., McEwan, A. G., and Thomson, A. J. (1992) Detection of the optical bands of molybdenum(V) in DMSO reductase (*Rhodobacter capsulatus*) by low-temperature MCD spectroscopy, *FEBS Lett. 307*, 169−172.
29. Zorin, N. A., Dimon, B., Gagnon, J., Gaillard, J., Carrier, P., and Vignais, P. M. (1996) Inhibition by iodoacetamide and acetylene of the H-D-exchange reaction catalyzed by *Thiocapsa roseopersicina* hydrogenase, *Eur. J. Biochem. 241*, 675−681.
30. Dixon, M. (1953) The determination of enzyme inhibitor constants, *Biochem. J. 55*, 170−171.
31. Cornish-Bowden, A., and Eisenthal, R. (1974) Statistical considerations in the estimation of enzyme kinetic parameters by the direct linear plot andother methods, *Biochem. J. 139*, 721−730.
32. Mouncey, N. J., and Kaplan, S. (1998) Cascade regulation of dimethyl sulfoxide reductase (dor) gene expression in the facultative phototroph *Rhodobacter sphaeroides* 2.4.1T, *J. Bacteriol. 180*, 2924−2930.
33. Karakas, E., Wilson, H. L., Graf, T. N., Xiang, S., Jaramillo-Busquets, S., Rajagopalan, K. V., and Kisker, C. (2005) Structural insights into sulfite oxidase deficiency, *J. Biol. Chem. 280*, 33506−33515.
34. Bartalesi, I., Bertini, I., Ghosh, K., Rosato, A., and Turano, P. (2002) The unfolding of oxidized c-type cytochromes: the instructive case of *Bacillus pasteurii*, *J. Mol. Biol. 321*, 693−701.
35. Barker, P. D., and Freund, S. M. (1996) Bis-methionine ligation to heme iron in mutants of cytochrome b562. 2. Characterization by NMR of heme-ligand interactions, *Biochemistry 35*, 13627−13635.
36. Romero, A., De la Cerda, B., Varela, P. F., Navarro, J. A., Hervas, M., and De la Rosa, M. A. (1998) The 2.15 A crystal structure of a triple mutant plastocyanin from the cyanobacterium *Synechocystis* sp. PCC 6803, *J. Mol. Biol. 275*, 327−336.
37. Williams, P. A., Blackburn, N. J., Sanders, D., Bellamy, H., Stura, E. A., Fee, J. A., and McRee, D. E. (1999) The CuA domain of *Thermus thermophilus* ba3-type cytochrome c oxidase at 1.6 A resolution, *Nat. Struct. Biol. 6*, 509−516.
38. D'Angelo, P., Pacello, F., Mancini, G., Proux, O., Hazemann, J. L., Desideri, A., and Battistoni, A. (2005) X-ray absorption

investigation of a unique protein domain able to bind both copper(I) and copper(II) at adjacent sites of the N-terminus of *Haemophilus ducreyi* Cu,Zn superoxide dismutase, *Biochemistry 44*, 13144−13150.
39. Jobling, M. F., Huang, X., Stewart, L. R., Barnham, K. J., Curtain, C., Volitakis, I., Perugini, M., White, A. R., Cherny, R. A., Masters, C. L., Barrow, C. J., Collins, S. J., Bush, A. I., and Cappai, R. (2001) Copper and zinc binding modulates the aggregation and neurotoxic properties of the prion peptide PrP106−126, *Biochemistry 40*, 8073−8084.
40. Mathys, W. (1975) Enzymes of heavy-metal resistant and non-resistant populations of *Silene cucubalus* and their interaction with some heavy metals in vitro and in vivo, *Physiol. Plant. 33*, 161−175.
41. Tripathi, B. N., Mehta, S. K., and Gaur, J. P. (2004) Recovery of uptake and assimilation of nitrate in *Scenedesmus* sp. previously exposed to elevated levels of Cu2+ and Zn2+, *J. Plant Physiol. 161*, 543−549.
42. Fischer, K., Barbier, G. G., Hecht, H. J., Mendel, R. R., Campbell, W. H., and Schwarz, G. (2005) Structural basis of eukaryotic nitrate reduction: crystal structures of the nitrate reductase active site, *Plant Cell 17*, 1167−1179.

BI700928M